

# Olfactory Network Differences in Master Sommeliers: Connectivity Analysis Using Granger Causality and Graph Theoretical Approach

Karthik Sreenivasan,<sup>1</sup> Xiaowei Zhuang,<sup>1</sup> Sarah J. Banks,<sup>1</sup> Virendra Mishra,<sup>1</sup> Zhengshi Yang,<sup>1</sup> Gopikrishna Deshpande,<sup>2-4</sup> and Dietmar Cordes<sup>1,5</sup>

## Abstract

Previous studies investigating the differences in olfactory processing and judgments between trained sommeliers and controls have shown increased activations in brain regions involving higher level cognitive processes in sommeliers. However, there is little information about the influence of expertise on causal connectivity and topological properties of the connectivity networks between these regions. Therefore, the current study focuses on addressing these questions in a functional magnetic resonance imaging (fMRI) study of olfactory perception in Master Sommeliers. fMRI data were acquired from Master Sommeliers and control participants during different olfactory and nonolfactory tasks. Mean time series were extracted from 90 different regions of interest (ROIs; based on Automated Anatomical Labeling atlas). The underlying neuronal variables were extracted using blind hemodynamic deconvolution and then input into a dynamic multivariate autoregressive model to obtain connectivity between every pair of ROIs as a function of time. These connectivity values were then statistically compared to obtain paths that were significantly different between the two groups. The obtained connectivity matrices were further studied using graph theoretical methods. In sommeliers, significantly greater connectivity was observed in connections involving the precuneus, caudate, putamen, and several frontal and temporal regions. The controls showed increased connectivity from the left hippocampus to the frontal regions. Furthermore, the sommeliers exhibited significantly higher small-world topology than the controls. These findings are significant, given that learning about neuroplasticity in adulthood in these regions may then have added clinical importance in diseases such as Alzheimer's and Parkinson's where early neurodegeneration is isolated to regions important in smell.

**Keywords:** effective connectivity; experts; functional magnetic resonance imaging; Granger causality; graph theory; olfaction

## Introduction

**F**UNCTIONAL AND STRUCTURAL brain changes have been reported in relation to training and expertise (experience-dependent plasticity) (Kolb et al., 2013) in humans. The studies looking for distinct structural changes have investigated diverse aspects of expertise, including juggling and associated motor and visual regions of the cortex, the hippocampal volume changes associated with taxi driving and spatial navigation training, cortical regions associated with language

learning in interpreters, structural changes (hippocampus and auditory cortex) with extensive musical training, and association of the frontal lobe olfactory regions with expertise in perfume (Bermudez and Zatorre, 2005; Delon-Martin et al., 2013; Oechslin et al., 2013; Valkanova et al., 2014).

Other studies have assessed the distinct pattern of functional activation in experts. For example, neural correlates of performance in archers (Kim et al., 2014), altered insula activation in expert meditators (Lutz et al., 2013), distinct patterns of olfactory regions and hippocampus activation in

<sup>1</sup>Cleveland Clinic Lou Ruvo Center for Brain Health, Las Vegas, Nevada.

<sup>2</sup>Department of Electrical and Computer Engineering, AU MRI Research Center, Auburn University, Auburn, Alabama.

<sup>3</sup>Department of Psychology, Auburn University, Auburn, Alabama.

<sup>4</sup>Alabama Advanced Imaging Consortium, Auburn University and University of Alabama Birmingham, Birmingham, Alabama.

<sup>5</sup>Department of Psychology and Neuroscience, University of Colorado, Boulder, Colorado.

perfumers when imaging smell (Plailly et al., 2012) and, during wine tasting, a functional magnetic resonance imaging (fMRI) study showed that wine experts (sommeliers) showed increased activation of the memory network (Pazart et al., 2014).

While many studies investigated structural or activation differences, there are few studies that examined the network-based connectivity differences related to expertise. Functional connectivity has been studied in musicians (Pinho et al., 2014), creative writers (Lotze et al., 2014), functional network organization in chess experts (Duan et al., 2014), and olfactory memory (Meunier et al., 2014). These studies investigate network-based functional connectivity. Despite the insights gained from these studies, they lack vital information related to the direction of the causal influence (effective connectivity). In high-level cognitive functioning and areas of expertise that are complex in nature, understanding information transfer among the brain regions involved in these processes could supplement the structural and functional findings and may provide valuable information about the neural networks involved in diverse areas of expertise.

Effective connectivity refers to the influence one neural system exerts over another, thus enabling us to find more information about how information flows between different brain regions. As a result, effective connectivity findings have added important information and yielded models of cognitive function by highlighting the extremely dynamic nature of the neural instantiations (McIntosh et al., 2010). Some of the more frequently used effective connectivity methods are dynamic causal modeling (DCM) (Friston et al., 2004), structural equation modeling (SEM) (McIntosh and Gozales-Lima, 1994), and Granger causality (GC) analysis (Abler et al., 2006; Deshpande et al., 2009; Roebroeck et al., 2005).

Unlike the confirmatory methods such as DCM and SEM, GC analysis is an exploratory technique that does not make any prior assumptions about the underlying connective architecture and is capable of obtaining condition-specific causal connectivity metrics between the larger number of brain regions using relatively shorter time series. Some of the earlier studies did examine causal connectivity differences related to learning using GC (Luo et al., 2012; Sathian et al., 2013), but such studies are few, and, to our knowledge, have not been completed on sommeliers (wine experts).

GC is based on the principle that the causal influence of one region X on another region Y can be obtained if past values of the time series from the region X help predict the present and future values of the time series from the region Y (Granger, 1969). This method is implemented using a multivariate autoregressive (MVAR) model. Several earlier studies have used these MVAR models based on the GC framework to study the predictive relationship between time series from different brain regions (Abler et al., 2006; Deshpande et al., 2011; Krueger et al., 2011; Lacey et al., 2011; Roebroeck et al., 2005).

However, it was shown that due to the effect of non-neuronal spatial variability of the shape of hemodynamic response functions (HRF) and slow sampling rate (Handwerker et al., 2004), using raw fMRI time series in GC analysis could lead to confounds in the estimation of causal connectivity metrics (David et al., 2008; Deshpande et al., 2010b). Consequently, recent studies have implemented an

improvised effective connectivity analysis framework. This framework implements blind hemodynamic deconvolution methods where in the underlying hidden neuronal variable for the fMRI time series can be estimated, and the GC analysis is done in the latent neuronal space (Grant et al., 2015; Hutcheson et al., 2015; Sathian et al., 2013).

The goals of this study are to investigate effective connectivity between brain regions in Master Sommeliers (wine experts) and untrained participants (nonwine experts) during olfactory tasks and study the global topological properties of these networks. In particular, we investigate the association between functional organization of the brain networks and the difference in olfactory expertise. Master Sommeliers undergo specialized training and have to pass a four-examination process that takes several years. By the end of their training, they have accumulated a wealth of knowledge linked to the smell of the wines. In addition to the obvious dependence on their sense of smell and taste, sommeliers also learn to draw on their memory and use mental imagery when judging wine. Therefore, we hypothesized that there would be network differences in effective connectivity and also the functional organization of the networks involving regions involved in olfaction, memory, multimodal integration, and mental imagery between Master Sommeliers and untrained controls. Furthermore, we also expected to see differences in the small-world topology in the effective connectivity networks in both groups.

In the current study, we explored the causal influences between different brain regions during olfactory fMRI tasks in trained Master Sommeliers and novice controls. Furthermore, the functional organization of the brain networks was studied using graph theoretical approaches, and the differences between the two groups were further statistically evaluated.

## Methodology

### Effective connectivity

**Blind deconvolution model.** The first step in the effective connectivity analysis is to deconvolve the HRF from the fMRI time series to obtain underlying neuronal response. In our article, we implement the blind deconvolution method proposed by Havlicek and colleagues (2011).

Let  $p$  fMRI time series be represented as  $Y(t)=[y_1(t) y_2(t) \dots y_p(t)]$ . A dynamic state-space model formulated in continuous time (discrete observation process) can be described as follows.

$$\tilde{n}_t^p = \begin{bmatrix} n_{\Gamma}^p \\ r_{\Gamma}^p \\ \theta_{\Gamma}^p \end{bmatrix} = \begin{bmatrix} f(n_{\Gamma-1}^p, r_{\Gamma-1}^p, \theta_{\Gamma-1}^p) \\ r_{\Gamma-1}^p \\ \theta_{\Gamma-1}^p \end{bmatrix} + \begin{bmatrix} L_{\Gamma-1}^p \\ K_{\Gamma-1}^p \\ J_{\Gamma-1}^p \end{bmatrix} \quad (1)$$

$$y_p(t) = m(\tilde{n}_t^p) + v_{t-1} \quad (2)$$

In the state equation [Eq. (1)],  $n$ ,  $r$ , and  $\theta$  are the neuronal state variables, the exogenous input, and the HRF parameter variables respectively. The symbol  $f$  is the function that links the current neuronal state to the previous state of  $n$ ,  $r$ , and  $\theta$ . The index  $\Gamma$  indicates continuous time, and  $L$ ,  $K$ , and  $J$  are the zero mean Gaussian state noise vectors. In the observation equation [Eq. (2)], the function  $m$  links the state variables and the measurement variables. The variables  $t$  and  $v$  represent the discrete time and measurement noise, respectively.

The exogenous input  $r$  (i.e., experimental boxcar function) and fMRI time series  $y_p(t)$  are the inputs to the model. The cubature Kalman filter (CKF) can be used to successfully estimate the hidden neuronal state variables and parameters. Briefly, this method uses an efficient joint scheme, in which the latent neuronal variables ( $n$ ) and the parameters corresponding to the HRF ( $\theta$ ) are combined into a single joint state vector and estimated together in a recursive manner by inverting a dynamic state-space model [Eqs. (1) and (2)]. For detailed explanation about this deconvolution method, the reader is referred to Havlicek and colleagues (2011).

Dynamic MVAR model. The neuronal state variables  $n_p(t)$  can be input into the MVAR as follows

$$\begin{bmatrix} n_1(t) \\ n_2(t) \\ \cdot \\ \cdot \\ n_p(t) \end{bmatrix} = \begin{bmatrix} 0 & a_{12}(0) & \cdots & a_{1p}(0) \\ a_{21}(0) & 0 & & a_{2p}(0) \\ \cdot & \cdot & 0 & \cdot \\ \cdot & \cdot & \cdot & \cdot \\ a_{p1}(0) & a_{p2}(0) & \cdots & 0 \end{bmatrix} \times \begin{bmatrix} n_1(t) \\ n_2(t) \\ \cdot \\ \cdot \\ n_p(t) \end{bmatrix} + \sum_{s=1}^{\omega} \begin{bmatrix} a_{11}(s) & a_{12}(s) & \cdots & a_{1p}(s) \\ a_{21}(s) & a_{22}(s) & & a_{2p}(s) \\ \cdot & \cdot & \cdot & \cdot \\ \cdot & \cdot & \cdot & \cdot \\ a_{p1}(s) & a_{p2}(s) & \cdots & a_{pp}(s) \end{bmatrix} \times \begin{bmatrix} n_1(t-s) \\ n_2(t-s) \\ \cdot \\ \cdot \\ n_p(t-s) \end{bmatrix} + \begin{bmatrix} \delta_1(t) \\ \delta_2(t) \\ \cdot \\ \cdot \\ \delta_p(t) \end{bmatrix} \quad (3)$$

Order of the model ( $\omega$ ) is determined by the Akaike/Bayesian information criterion (Akaike, 1974; Schwarz, 1978),  $a$  are the model coefficients and  $\delta$  is the model error. Note that  $a(0)$  and  $a(s)$ ,  $s=1 \dots \omega$  represent the instantaneous influences between time series and causal influences between time series, respectively. By modeling both these terms in the model, the effect of instantaneous correlation on causality can be minimized (Deshpande et al., 2010a). By varying the model coefficients as a function of time, the MVAR model can be made dynamic, as given below [Eq. (4)].

$$\begin{bmatrix} n_1(t) \\ n_2(t) \\ \cdot \\ \cdot \\ n_p(t) \end{bmatrix} = \begin{bmatrix} 0 & a_{12}(0,t) & \cdots & a_{1p}(0,t) \\ a_{21}(0,t) & 0 & & a_{2p}(0,t) \\ \cdot & \cdot & 0 & \cdot \\ \cdot & \cdot & \cdot & \cdot \\ a_{p1}(0,t) & a_{p2}(0,t) & \cdots & 0 \end{bmatrix} \times \begin{bmatrix} n_1(t) \\ n_2(t) \\ \cdot \\ \cdot \\ n_p(t) \end{bmatrix} + \sum_{s=1}^{\omega} \begin{bmatrix} a_{11}(s,t) & a_{12}(s,t) & \cdots & a_{1p}(s,t) \\ a_{21}(s,t) & a_{22}(s,t) & & a_{2p}(s,t) \\ \cdot & \cdot & \cdot & \cdot \\ \cdot & \cdot & \cdot & \cdot \\ a_{p1}(s,t) & a_{p2}(s,t) & \cdots & a_{pp}(s,t) \end{bmatrix} \times \begin{bmatrix} n_1(t-s) \\ n_2(t-s) \\ \cdot \\ \cdot \\ n_p(t-s) \end{bmatrix} + \begin{bmatrix} \delta_1(t) \\ \delta_2(t) \\ \cdot \\ \cdot \\ \delta_p(t) \end{bmatrix} \quad (4)$$

The model coefficients  $a_{ij}(s,t)$  were taken as the state vector of a Kalman filter and adaptively estimated using the algorithm proposed by Arnold and colleagues (1998). Dynamic GC was then obtained as follows.

$$DGC_{ij}(t) = \sum_{s=1}^{\omega} [a_{ij}(s,t)] \quad (5)$$

In Equation (5), the model coefficients obtained are summed over all orders of the model. This enables us to infer net (effective) causality between the time series.

**Graph theory analysis**

The topological properties of functional networks were investigated by graph theoretical analysis. The causal connectivity matrices obtained from the connectivity model were

used for the analysis. Each matrix was thresholded into a set of weighted graphs (i.e., networks) by selecting the strongest connections until the desired sparsity was reached. Connection sparsity ( $S$ ; ratio of the existing edges to the maximum possible number of edges in a network) was used as a thresholding measure in the current study. The threshold was applied to ensure that the networks being compared had the same number of nodes and edges to analyze between-group differences in the network organization (Achard and Bullmore, 2007). A threshold range of  $0.10 < S < 0.50$  with an interval of 0.01 was applied to each connectivity matrix. This range of sparsity was chosen as it is comparable to the range indicated in prior studies (He et al., 2008; Rubinov and Sporns, 2010). The following network analysis was repeatedly performed on this defined threshold range.

At each  $S$ , we obtained network characteristics, including (1) small-world parameters and (2) network efficiency. Small-world properties were originally proposed by Watts and Strogatz (1998). It involved determination of weighted clustering coefficient ( $C$ ), weighted characteristic path length ( $L$ ), normalized weighted clustering coefficient ( $C_N$ ), and normalized weighted characteristic path length ( $L_N$ ). The  $C$  of a network quantifies the degree of local interconnectivity in a network and is expressed as the average of clustering coefficients across all nodes in the network:  $C = \frac{1}{N} \sum_{i \in N} C_i$ , where  $N$  and  $C_i$  denote the number of nodes and the clus-

tering coefficient of node  $i$ , respectively. The clustering coefficient of a node is defined as the likelihood that the neighborhoods of node  $i$  are connected to each other and is given by Equation (6)

$$C_i = \sum_{j,h \in N} \frac{(w_{ij}w_{ih}w_{jh})^{\frac{1}{3}}}{2(e_i(e_i-1) - 2 \sum_{j \in N} a_{ij}a_{ji})} \quad (6)$$

where  $e_i$  is the number of edges connecting to node  $i$  (degree<sub>in+out</sub>),  $w_{ij}$  is the connectivity value between node  $i$  and node  $j$ , and  $a_{ij}$  is the connection status between the nodes. The  $C$  quantifies the extent of local interconnectivity or cliquishness in network (Onnela et al., 2005; Watts and Strogatz, 1998). The path length between node  $i$  and node  $j$  was defined as the sum of edge length along this path. The length of each edge was calculated as the

reciprocal of edge weight ( $1/w_{ij}$ ). The path length  $L_{ij}$  was defined as the length of the shortest path between node  $i$  and node  $j$ :  $L_{ij} = \sum_{a_{uv} \in g_{i \rightarrow j}} \left( \frac{1}{w_{uv}} \right)$ , where  $g_{i \rightarrow j}$  is the shortest weighted path between  $i$  and  $j$ . The weighted characteristic path length (Rubinov and Sporns, 2010) is given by Equation (7)

$$L = \frac{1}{N} \sum_{i \in N} \frac{\sum_{j \in N, j \neq i} L_{ij}}{N-1} \quad (7)$$

A network is considered small world if it has similar path length but higher local connectivity than random networks (Watts and Strogatz, 1998). The small worldness of a network can be expressed as  $s = C_N/L_N$ , which is typically larger than 1 in the case of small-world organization ( $C_N = C/C_{\text{random}} > 1$  and  $L_N = L/L_{\text{random}} \sim 1$ ) (Achard et al., 2006; Watts and Strogatz, 1998). The mean weighted clustering coefficient and weighted characteristic path length of 100 matched random networks are given by  $C_{\text{random}}$  and  $L_{\text{random}}$ . The random networks are matched to preserve the same number of nodes, edges, and degree distribution as the real network.

To study the network efficiency, we obtained the local ( $E_{\text{local}}$ ) and global efficiency ( $E_{\text{global}}$ ) of the connectivity networks. The efficiency is a measure of how well a network exchanges information (Achard and Bullmore, 2007). Global efficiency quantifies the exchange of information on a global scale in the network and the local efficiency is a measure of how well local subgraphs exchange information when the node under consideration is eliminated. All of the above network measures were calculated using the appropriate functions provided in the Brain Connectivity Toolbox (Rubinov and Sporns, 2010).

To evaluate the between-group differences in overall topological characteristics, we calculated the area under the curve (AUC) over the whole range of thresholds. The AUC provides a summarized scalar for topological characterization of brain networks independent of single threshold selection (Achard and Bullmore, 2007). The integrated AUC of network metric  $Y$ , which was computed over the threshold range of  $S_1 = 0.1$  and  $S_n = 0.50$  with interval of  $\Delta S = 0.01$ , was expressed as follows [Eq. (8)]:

$$Y_{\text{AUC}} = \sum_{l=1}^{n-1} [Y(S_l) + Y(S_{l+1})] \frac{\Delta S}{2} \quad (8)$$

## Materials and Methods

### Subjects

A total of 26 healthy adults participated in the study. Thirteen Master Sommeliers (11 male, 2 female; age:  $44.42 \pm 10.2$  years; years as Master Sommelier:  $8.92 \pm 7.4$ ) and 13 controls (11 male, 2 female; age:  $34 \pm 5.8$  years). All methodology was reviewed and approved by the Cleveland Clinic Institutional Review Board (IRB) for the imaging study. Informed consent was obtained from all participants before taking part in the study.

Master Sommeliers were recruited from the Las Vegas resort community and surrounding regions by S.J.B. with the assistance of Jay James, a Master Sommelier extensively involved in both training of sommeliers and in the local community. Control participants were recruited via advertising

and word of mouth from among the local professional and academic community at the University of Nevada, Las Vegas. A 10-item multiple-choice wine quiz was developed to assess the extent of wine knowledge in the controls. Controls who scored 30–90% (mean of 64%) were included in the study since they were not likely to have a higher level of wine-related knowledge than most of the nonsommelier population and less likely to be considered as a naive control group.

### Overview of the olfactory imaging system

Before entering the scanner, subjects were fitted with a modified medical-grade oxygen face mask. The custom mask was modified to accommodate the placement of eight polyurethane tubes immediately below the nose. A small glass bottle was attached to the end of each of the tubes. The bottles contained a small amount (4 mL) of either wine (two red and two white wine bottles), or nonwine (three bottles), or nothing (one bottle). Additional tubing from each of these bottles connected them to the olfactometer. The olfactometer is a computer-controlled pneumatic stimulator (Institute for Biomagnetism and Biosignal analysis, University of Munster, Germany) that provides air pulses of well-defined duration. The apparatus are depicted in Figure 1.

### Experimental stimuli

The entire study consisted of 2 runs of 80 trials and lasted  $\sim 20$  min. Two olfactory and two nonolfactory were presented pseudorandomly in an event-related design. There was a 2-sec visual cue at the beginning of each trial informing participants which task to perform during the subsequent stimulus presentation that lasted 4 sec. The fixation period between the trials varied from 0 to 5500 ms. By using a pseudorandomized stimulus presentation, we were able to ensure that there were sufficient intervals between olfactory stimulus presentations to allow for recovery of the olfactory system and to avoid the effects of habituation. Figure 2 illustrates the timing and tasks.

During the olfactory tasks, a single odorant was presented. The participants were instructed to smell and were informed as to which olfactory task to perform. Odorants were delivered for 4 sec. For one of the olfactory tasks, participants reported whether the odorant was red or white wine, and for the other, they reported if the odorant presented was a wine or a nonwine. For the olfactory tasks, two white wines, two red wines, and three nonwine mixtures (a blend of white verjus with a small amount of vodka, and some combination of fresh lemon juice and very dilute pear or apricot essence) were chosen. Wines were opened, and nonwines mixed fresh, for each imaging session, with a maximum of three participants being run in a session.

One of the nonolfactory task was a motor task, where the participants received a 4-sec stream of air through an olfactometer channel that contained no odorant and were asked to respond by arbitrarily pressing the left or right button. The other nonolfactory task was a visual discrimination task during which participants were randomly presented a pixelated image of a fingerprint or zebra pattern and were asked whether the image was a fingerprint or a zebra pattern.

### Data acquisition

All images were acquired on a Siemens Verio 3 Tesla MRI scanner with a birdcage head coil. A high-resolution

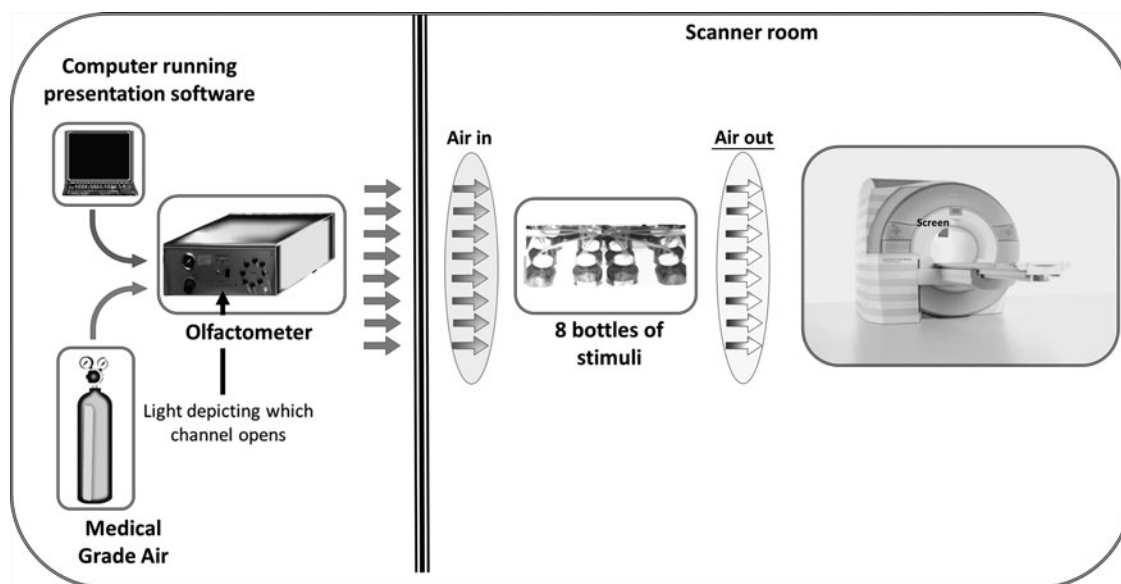


**FIG. 1.** Apparatus during scanning. Medical-grade air enters the olfactometer, which controls release of air into one of eight channels, opened when instructed by the presentation program. The air then travelled in a tube to one of eight bottles, seven of which included either wine or nonwine liquid. The other was empty. The air then went in a different tube to the mask attached to the face of the participant.

( $1 \times 1 \times 1.2$  mm) structural image was acquired using a T1-weighted gradient echo 3D MP-RAGE sequence (repetition time [TR]=2300 ms, echo time [TE]=2.98 ms, flip angle=9°). The structural scan was of no importance to the analysis in this study. Functional scans were acquired using gradient echo T2\*-weighted echo planar imaging (EPI), optimized for BOLD (blood oxygen level dependent) contrast. Imaging parameters were TR=2500 ms, TE=28 ms, flip angle=80°, field of view=256 mm; slice thickness 4 mm; in-plane resolution=2×2 mm. A total of 240 volumes were obtained during each of 2 trial sessions.

*Data analysis*

FMRI data were preprocessed using SPM12. All the statistical analyses were performed using MATLAB 2015a. EPI data were input into a standard preprocessing pipeline that performed slice time correction, realignment, coregistration, and normalization to the Montreal Neurological Institute (MNI) 2 mm template. Finally, data were smoothed with an 8 mm Gaussian kernel. Ninety different cortical regions of interest (ROIs; excluding cerebellum) were identified based on the Automated Anatomical Labeling atlas

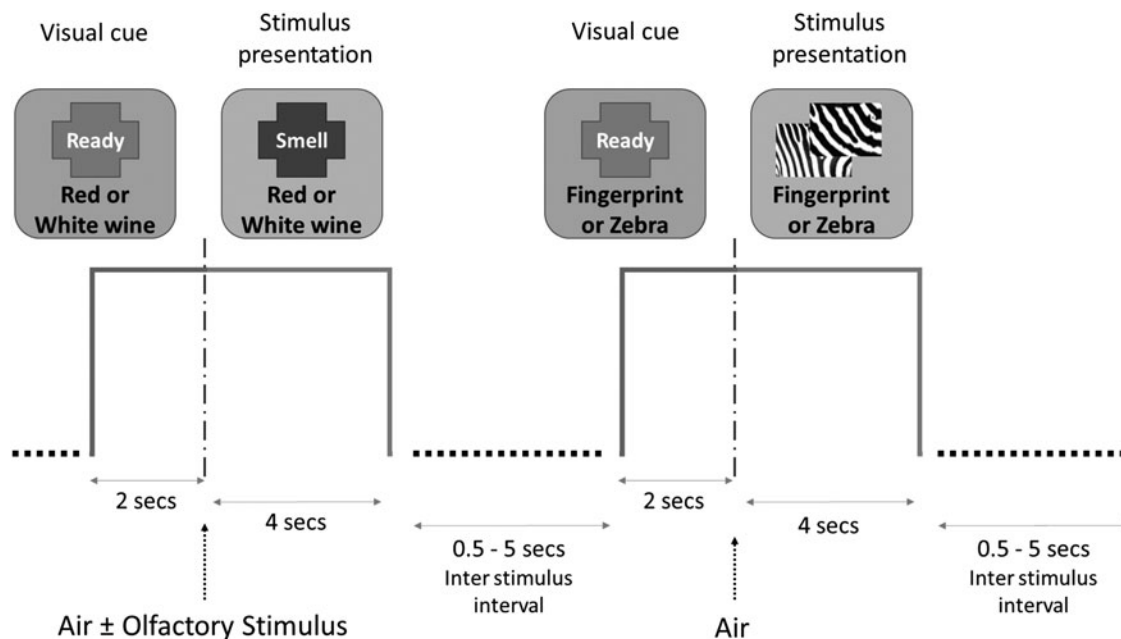


**FIG. 2.** Example of two stimulus presentations showing an olfactory stimulus (red or white wine) and a visual stimulus (fingerprint or zebra).

(Tzourio-Mazoyer et al., 2002). No global signal regression was performed (Aguirre et al., 1998; Glasser et al., 2013; Murphy et al., 2009). Average time series were extracted from these regions for all participants. These average time series were standardized and then the latent neuronal state

variables were obtained by hemodynamic deconvolution of the fMRI time series using the CKF. A boxcar function corresponding to the input stimulus was used as the exogenous input to the deconvolution model along with normalized fMRI time series from previously identified activated

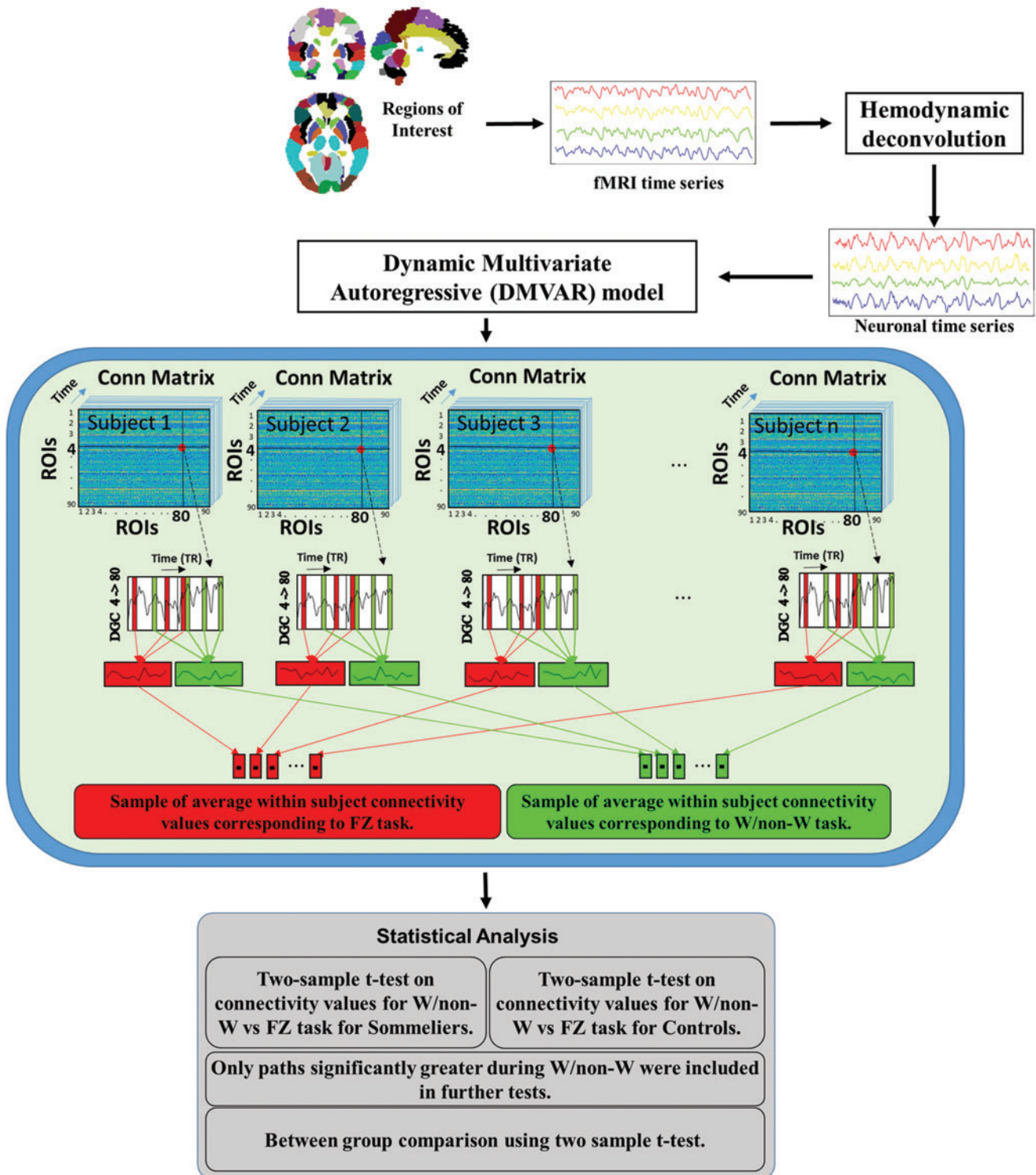


**FIG. 3.** Schematic displaying the processing pipeline for the connectivity analysis. The dot indicates the connection or path between two regions. The black lines that cross this dot point to the regions on the x and y axis. The dashed arrow is pointing to the window displaying the dynamic causality values (connectivity over time) for the connection. Color images available online at [www.liebertpub.com/brain](http://www.liebertpub.com/brain)

ROI. The hidden neuronal variables obtained after deconvolution were input into a dynamic MVAR model (model order 4) to obtain dynamic effective connectivity between every pair of ROI for all the participants. Samples of task-specific connectivity were then obtained for each participant by populating the absolute causality values at the time point corresponding to wine or nonwine and the fingerprint or zebra pattern conditions. These were averaged within subject and task-specific connectivity values were then obtained for all participants (Fig. 3 middle panel).

Two-sample *t*-tests were performed between these samples (within each group) and paths that were significantly ( $p < 0.05$ ) greater during the wine/nonwine task, when compared to the fingerprint/zebra task, were identified. The fingerprint/zebra task was chosen as the control or baseline condition because (1) visual judgment skill differences are minimal between the two groups; (2) comparing the olfactory task and the complex visual discrimination task enables

us to study the processes involving olfactory ability of the sommeliers rather than perceptual judgment in general.

For the paths identified above, the connectivity values during the wine/nonwine task were obtained for the two groups and then compared (between the groups) using a two-sample *t*-test (controlling for age and gender) to identify the causal connections that were significantly different between sommeliers and controls. The schematic of the data analysis pipeline is shown in Figure 3. We performed a linear regression analysis between the mean connectivity value of all the paths that were greater in sommelier during olfaction and their experience (years as Sommelier) and reaction time (RT; during the wine/nonwine task) with gender and age as covariates.

*Graph theory analysis*

The connectivity matrices obtained from the MVAR model were further used to calculate the small worldness

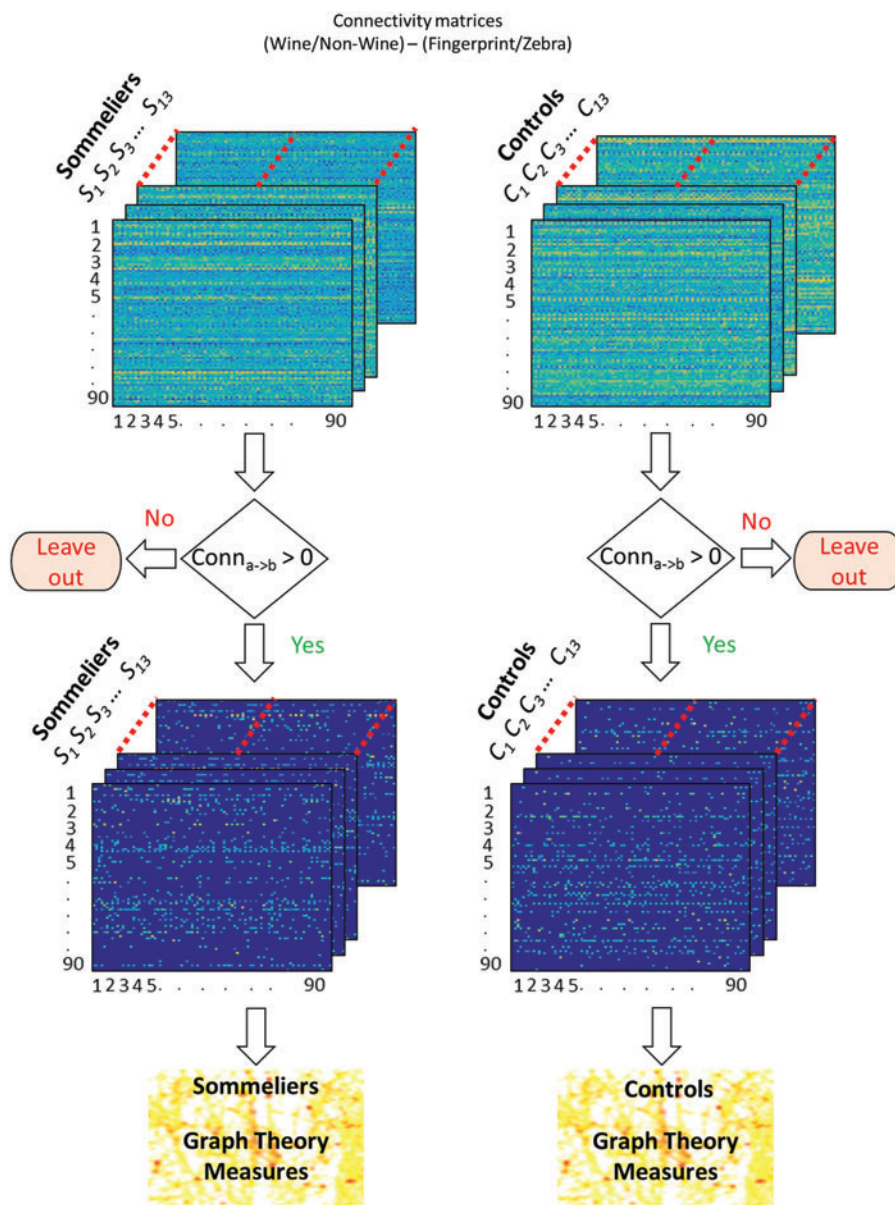
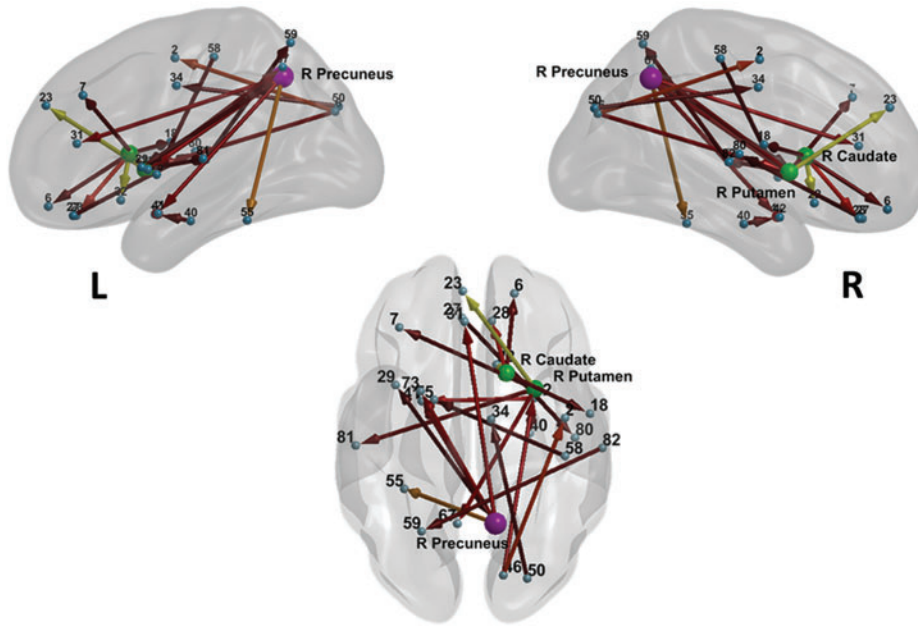


**FIG. 4.** Schematic displaying the processing pipeline for the graph theory analysis. The paths that had wine/nonwine connectivity < fingerprint zebra connectivity were left out at the decision step. Color images available online at [www.liebertpub.com/brain](http://www.liebertpub.com/brain)

**a**

Sommeliers > Control



- 2 – Right Precentral
- 6 – Right Sup. Orb. Frontal
- 7 – Left Mid. Frontal
- 18 – Right Rolandic Oper.
- 22 – Right Olfactory
- 23 – Left Sup. Med. Frontal
- 27 – Left Gyrus Rectus
- 28 – Right Gyrus Rectus
- 29 – Left Insula
- 31 – Left Ant. Cingulum
- 34 – Right Mid. Cingulum
- 40 – Right ParaHipp.
- 41 – Left Amygdala
- 42 – Right Amygdala
- 46 – Right Cuneus
- 50 – Right Supp. Occipital
- 55 – Left Fusiform
- 58 – Right Postcentral
- 59 – Left Sup. Parietal
- 67 – Left Precuneus
- 73 – Left Putamen
- 75 – Left Pallidum
- 80 – Right Heschl
- 81 – Left Sup. Temporal
- 82 – Right Sup. Temporal

**b**

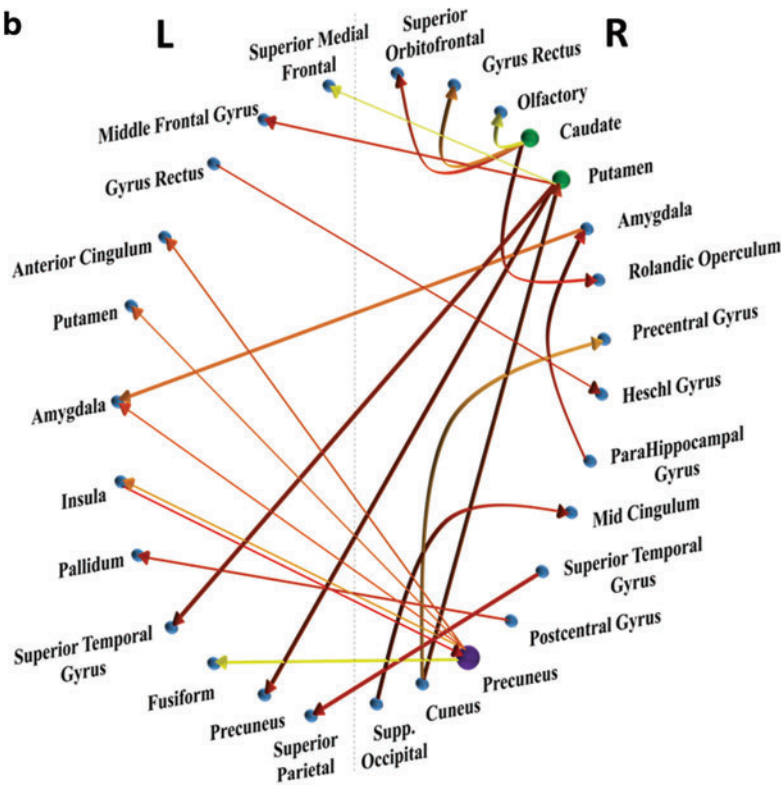


**FIG. 5.** Paths significantly greater in the sommeliers when compared to controls during the wine/nonwine task. **(a)** Shows a glass brain representation of the paths visualized using BrainNet Viewer (Xia et al., 2013) and **(b)** shows a circle plot displaying the paths. The color of the connections indicate least significant (red; 0) to most significant (yellow; 1). The purple node has the highest out degree (5) and the green nodes have the second highest out degree (4). The other nodes have out degree <4. Color images available online at [www.liebertpub.com/brain](http://www.liebertpub.com/brain)

and global and local efficiencies of the network for all the participants. These graph theory measures were obtained at different sparsity levels. A difference matrix was obtained for each subject by subtracting the fingerprint/zebra task connectivity values from the wine/nonwine task connectivity values. One-sample *t*-tests (right tailed) were used on these new connectivity values (wine/nonwine connectivity—fingerprint zebra connectivity) and the *t*-values were obtained. This *t*-value was used as a threshold to choose the strongest causal connections until a desired sparsity was reached. As mentioned earlier, a sparsity threshold range of  $0.1 < S < 0.50$  with an interval of 0.01 was applied to each connectivity matrix. Figure 4 shows a schematic of the graph theory analysis pipeline. The integrated AUC graph theory metrics over the different sparsity thresholds for the two groups were obtained. The samples were then compared using *t*-test (controlling for age and gender) to obtain the between-group differences in network topology.

**Results**

The results of this study are summarized as follows: (1) there were 28 effective connectivity paths that were significantly different between sommeliers and controls and (2) there were enhanced small-world organization and significantly greater clustering coefficient and smaller path length in the sommeliers when compared to untrained participants.

The first set of results is associated with the identification of important effective connectivity paths that are different between the Master Sommeliers and the untrained participants. The results show 28 significantly different paths between the 2 groups during the olfactory task. Twenty-two of these paths were significantly greater ( $p < 0.05$ , Cohen’s *d* [effect size]  $> 0.7$ ) in sommeliers during the wine/nonwine task and six of the connections were greater in controls. The

results were visualized using BrainNet Viewer (Xia et al., 2013, www.nitrc.org/projects/bnv/). Figure 5 and Table 1 show the effective connectivity paths to be significantly greater in the sommeliers compared to untrained controls. We see significantly greater connectivity in sommeliers, mainly comprising connections involving the precuneus, caudate, putamen, and several frontal and temporal regions ( $p < 0.05$ , Cohen’s *d* [effect size]  $> 0.7$ , Fig. 5 and Table 1).

Figure 6 and Table 2 show paths that were significantly greater in untrained participants when compared to the sommeliers, which primarily involve connections from the left hippocampus to the frontal regions ( $p < 0.05$ , effect size  $> 0.7$ ).

Second, the graph theory analysis results showed that both the sommeliers and the control group represented a small-world organization for the defined range of sparsity thresholds (*S*). Furthermore, comparing the integrated AUC values, we found that the sommeliers had significantly greater small worldness ( $\sigma$ ;  $p = 7.54 \times 10^{-5}$ ) and normalized weighted clustering coefficient ( $\gamma$ ;  $p = 1.69 \times 10^{-11}$ ) when compared to the untrained controls (Fig. 7). There were no significant differences in the normalized weighted characteristic path length ( $\lambda$ ), global efficiency ( $E_{glob}$ ), and the local efficiency ( $E_{loc}$ ).

There were no statistically significant findings when assessing relationship between connectivity and years of experience as a sommelier or RT during the wine/nonwine task. However, these findings did exhibit expected trends with connectivity, showing a positive relationship with experience and an inverse relationship with RT with a moderate effect size (Cohen’s *d*  $> 0.6$ ) (Fig. 8).

**Discussion**

To our knowledge, this is the first study to use causal connectivity measures to investigate the high-level cognition

TABLE 1. PATHS SIGNIFICANTLY GREATER IN THE SOMMELIERS THAN CONTROLS DURING THE WINE/NONWINE TASK WITH THEIR CORRESPONDING *p*-VALUES AND EFFECT SIZE

	Source	→	Sink	p	Effect size
Sommeliers > controls	Rectus L	→	Heschl R	0.049	0.75
	Insula L	→	Precuneus R	0.049	0.75
	Parahippocampal R	→	Amygdala R	0.041	0.80
	Amygdala R	→	Amygdala L	0.013	1.04
	Cuneus R	→	Precentral R	0.009	1.13
	Cuneus R	→	Putamen R	0.025	0.91
	Occipital superior R	→	Cingulum mid R	0.047	0.76
	Postcentral R	→	Pallidum L	0.046	0.77
	Precuneus R	→	Insula L	0.007	1.17
	Precuneus R	→	Cingulum anterior L	0.024	0.91
	Precuneus R	→	Amygdala L	0.027	0.89
	Precuneus R	→	Fusiform L	0.005	1.23
	Precuneus R	→	Putamen L	0.023	0.93
	Caudate R	→	Frontal superior orbital R	0.038	0.82
	Caudate R	→	Rolandic operculum R	0.041	0.80
	Caudate R	→	Olfactory R	0.002	1.39
	Caudate R	→	Rectus R	0.011	1.09
	Putamen R	→	Frontal mid L	0.043	0.79
	Putamen R	→	Frontal superior medial L	0.001	1.60
	Putamen R	→	Precuneus L	0.028	0.88
	Putamen R	→	Temporal superior L	0.033	0.85
	Temporal Superior R	→	Parietal superior L	0.039	0.81

L, left; R, right.

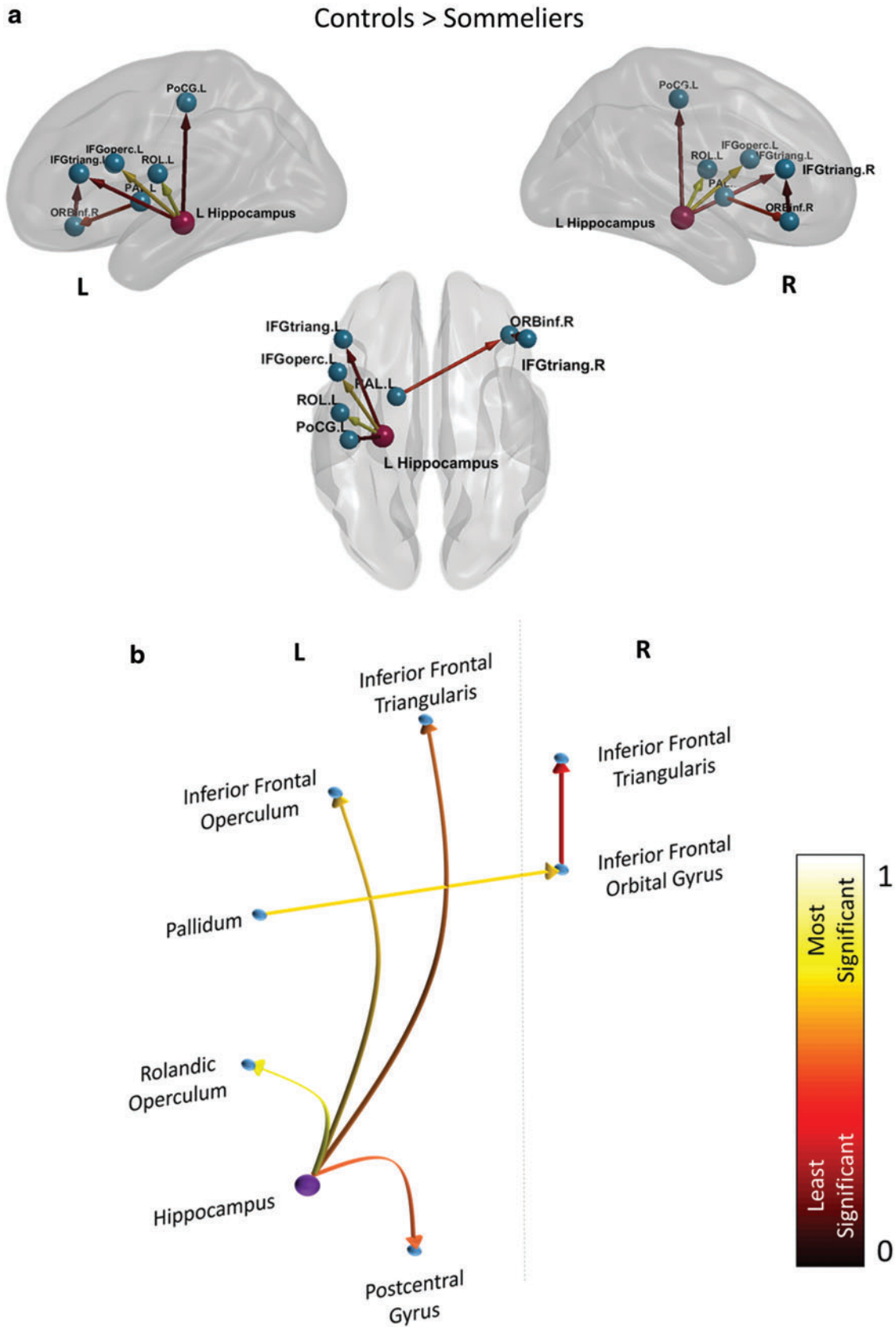


TABLE 2. PATHS SIGNIFICANTLY GREATER IN THE CONTROLS THAN SOMMELIERS DURING THE WINE/NONWINE TASK WITH THEIR CORRESPONDING *p*-VALUES AND EFFECT SIZE

	Source	→	Sink	p	Effect size
Controls > sommeliers	Frontal inferior orbital R	→	Frontal inferior triangularis R	0.046	0.77
	Hippocampus L	→	Frontal inferior operculumsss L	0.009	1.12
	Hippocampus L	→	Frontal inferior triangularis L	0.034	0.84
	Hippocampus L	→	Rolandic operculum L	0.004	1.28
	Hippocampus L	→	Postcentral L	0.043	0.78
	Pallidum L	→	Frontal inferior orbital R	0.018	0.98

during olfaction in sommeliers. The findings of this study were (1) sommeliers showed significantly increased connectivity involving the precuneus, caudate, putamen, and several frontal and temporal regions, while there was an increased connectivity in paths primarily involving connections from the left hippocampus to the frontal regions in controls and (2) the sommeliers showed significantly greater small worldness when compared to the controls.

*Effective connectivity differences between sommeliers and controls*

There were 28 effective connectivity paths that were significantly different (after controlling for age and gender) between the 2 groups, with 22 paths showing increased connectivity in sommeliers and 6 paths in untrained controls. In the untrained participants, majority of the connections were from the left hippocampus to the frontal regions. This particular finding that the major node of connectivity in untrained participants was located in the left hippocampus is perhaps surprising in view of previous work indicating the role of left hippocampus for context-dependent memory (Frisk and Milner, 1990). It is well known that the hippocampus is essential for learning and memory retrieval in humans (Miller and D’Esposito, 2012). Specifically, in olfaction, the hippocampus plays a role in creation of mental images of odors, memory, and the formation of complex sensory associations (Royet et al., 2013; Saive et al., 2014). However, as previously noted by Royet and colleagues (2013), olfactory ex-

perts showed lesser involvement of the hippocampus and other key regions involved in olfaction and odor-specific memory or associations with a greater level of expertise. Hence, we assume that in the absence of any formal training, the control participants responded based on their past experience thus recruiting the left hippocampus as a major node in their connectivity network.

In sommeliers, increased connectivity was observed in paths and regions that are found to be part of the olfactory network. Several nodes, such as the olfactory cortex, insula, amygdala, parahippocampal gyrus, operculum, and putamen, have been associated with processing odor identification and gustatory and sensory networks in earlier studies (Castriota-Scanderbeg et al., 2005; Pazart et al., 2014; Royet et al., 2013). Our results also include significant functional alterations in brain regions (precuneus, caudate, and putamen) involved in high-level cognition network (e.g., attention, mental imagery, working memory). These three regions were the major connectivity nodes in the sommeliers (Fig. 5 and Table 1).

Given our study and the nature of task (odor recognition and discrimination), the identification of paths involving these regions is consistent with earlier studies that have shown their involvement in executive functioning and working memory. The dorsal striatum (putamen and caudate) contribute directly to decision-making by integrating sensorimotor, cognitive, and emotional information (Balleine et al., 2007). The other major node, the right precuneus, is shown to be involved in episodic memory retrieval, mental imagery recall, and retrieval independent of imagery (Lundstrom et al., 2005).

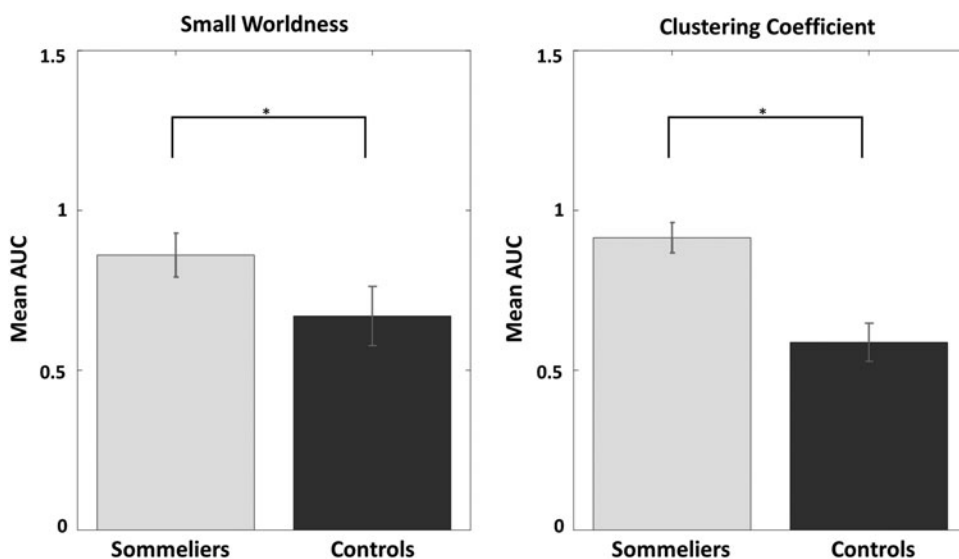
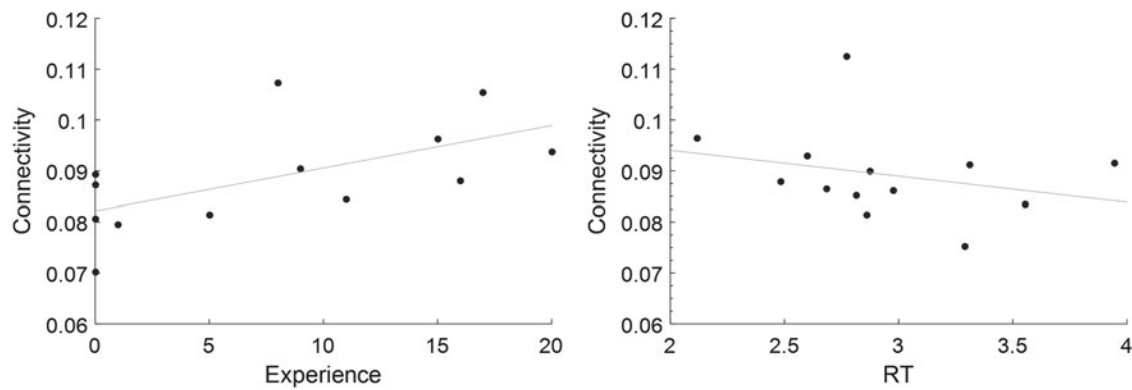


FIG. 7. Between-group differences in graph theory metrics during the wine/nonwine task. The bar plots indicate the statistical difference of integrated AUC over a range of sparsity thresholds (S) between the sommeliers and the untrained controls. AUC, area under the curve.



**FIG. 8.** Plots showing the interaction between mean connectivity values of all paths greater in sommelier during olfaction and experience (years as Master Sommelier) and RT during the wine/nonwine task. The y-axis represents connectivity values after regressing out the age and gender. RT, reaction time.

Moreover, specific to olfactory functions, Savic and colleagues (2000) studied cerebral activations with positron emission tomography during five different olfactory tasks (each with varied levels of cognitive demands corresponding to odor perception, discrimination, and recognition memory) and showed involvement of different sets of brain regions. In that study, the authors showed involvement of the putamen and caudate in odor identification, the caudate also played a role in odor quality discrimination, and the precuneus was one of the regions that showed increased activation in odor recognition memory, supporting the findings of this study (Fig. 5).

Although olfactory functions involve many other regions such as the olfactory cortex, amygdala/piriform cortex, right orbitofrontal cortex, and insular/peri-insular cortex (Savic et al., 2000), we did not see connectivity differences in many of these brain regions involved in olfactory processing between the two groups. One possible explanation for this is, activities that sommeliers practice throughout their learning and work depend on regions involved in high-level cognition such as mental imagery, sensory integration, and working memory systems to identify wines. Therefore, significant differences were seen in regions involved in multisensory integration and higher order cognitive processes rather than the primary olfactory regions.

#### *Difference in small worldness in sommeliers and controls*

Previous studies have shown that the functional connections of the brain networks are structured in an extremely well-organized small-world manner (Achard et al., 2006; Sporns et al., 2004; Van den Heuvel et al., 2008). This small-world organization is characterized by a high level of local interconnectivity or local clustering, which is responsible for efficient local information processing, as well as existence of efficient long-distance connections (with a short average path between nodes) that ensure a high level of global communication efficiency and integration of information within the overall network (Bullmore and Sporns, 2009; Watts and Strogatz, 1998). In other words, we could say that a small-world organization reflects an optimized network organization, which could be in turn associated with difference in cognition.

Our results show that both the sommeliers and the controls have an efficient small-world organization of the brain network ( $\sigma > 1$ ), but the Master Sommeliers have a significantly greater small-world index ( $\sigma$ ) and normalized clustering coefficient ( $\gamma$ ) when compared to untrained controls. Studies have shown that training and expertise enhance the network characteristics (Duan et al., 2014; Van den Heuvel et al., 2009; Voss et al., 2010). Therefore, we attribute this enhancement in network organization to the rigorous learning experienced by the Master Sommeliers. The graph theory findings of this study suggest reorganization of the brain networks in Master Sommeliers during olfaction, which may be attributed to the expertise.

This study is unique because we investigated effective connectivity and topological properties of brain organization in Master Sommeliers, a population of experts who have a distinctive skill set and the population is small. There are 230 professionals (147 Master Sommeliers in America's chapter) worldwide who have received the title of Master Sommelier since the organization's inception ([www.mastersommeliers.org/about#](http://www.mastersommeliers.org/about#)). By including only individuals with this distinction, we could be assured that we were assessing true experts. Although we were able to recruit all the Master Sommeliers from the Las Vegas resort community and surrounding regions, the sample size is still small due to the rare profession. Despite working with a limited sample, our results show a large effect size, therefore upholding the statistical significance of our findings. Given the restrictions in the size of the expert population, future studies might need to be multisite in nature to gain access to a larger pool of Master Sommeliers. This may allow the detection of significant relationship between connectivity and behavior that were not observed in the current data set.

Another important aspect of olfactory research is that most, if not all, odorants activate both the olfactory and the trigeminal system (Doty et al., 1978; Frasnelli et al., 2011). Investigating this overlap of activation between the olfactory and trigeminal system is not within the scope of the current study. However, by including alcohol in the nonwine mixtures, we ensured that there was similar trigeminal stimulation across olfactory stimulus so that the difference in connectivity could be attributed to olfactory judgment and not to the degree of activation of either (olfactory or trigeminal) of these systems.

## Conclusions

The current study used fMRI to investigate differences in effective connectivity and network topology between a group of trained Master Sommeliers and untrained control participants during olfactory tasks. Master Sommeliers showed stronger connectivity originating from regions of the brain involved in higher level cognitive processes, when compared to untrained controls. There was also increased small-world topology in the sommeliers. This increase in connectivity and enhanced network reorganization can be attributed to the rigorous learning undertaken by the Master Sommeliers. Our findings provide unique insights into the neuroplasticity of the brain in adulthood and further the understanding related to influence of higher level cognitive learning on efficient organization of functional networks in the brain. These findings may have added clinical importance in diseases such as Alzheimer's and Parkinson's, where the earlier neurodegeneration is isolated to regions important in smell and early interventions to alter these networks could help slow the disease.

## Acknowledgments

Our gratitude is extended to the sommeliers and control participants. This study was partially supported by grant funding from the National Institute of General Medical Sciences (grant: P20GM109025). This study was also funded via the Director's Innovation Fund, and we thank Dr. Jeffrey Cummings for making the funds available. We thank Fusion and Mr. Larry Ruvo at Southern Wine and Spirits for donation of verjus and wine, respectively, to the study. We further thank Dr. Johannes Frasnelli, Dr. Steve Rao, and Sally Dugerman for their input on the fMRI study design. Dr. Gabriel Leger conceived of the original study design along with Dr. Banks, and was instrumental in the design and implementation of the original study. We thank Jay James, Dr. Erik Beall, David Weintraub, Deanna Baldock, Michael Noback, and Meghan Pierce for assisting with implementation of the original study.

## Author Disclosure Statement

No competing financial interests exist.

## References

- Abler B, Roebroek A, Goebel R, Hose A, Schfnfeldt-Lecuona C, Hole G, et al. 2006. Investigating directed influences between activated brain areas in a motor-response task using fMRI. *Magn Reson Imaging* 24:181–185.
- Achard S, Bullmore E. 2007. Efficiency and cost of economical brain functional networks. *PLoS Comput. Biol* 3:e17.
- Achard S, Salvador R, Whitcher B, Suckling J, Bullmore E. 2006. Aresilient, low-frequency, small-world human brain functional network with highly connected association cortical hubs. *J Neurosci* 26:63–72.
- Aguirre GK, Zarahn E, D'Esposito M. 1998. The inferential impact of global signal covariates in functional neuroimaging analyses. *Neuroimage* 8:302–306.
- Akaike H. 1974. A new look at the statistical model identification. *IEEE Trans Autom Control* 19:716–723.
- Arnold M, Miltner W, Witte H, Bauer R, Braun C. 1998. Adaptive AR modeling of nonstationary time series by means of Kalman filtering. *IEEE Trans Biomed Eng* 45:553–562.
- Balleine BW, Delgado MR, Hikosaka O. 2007. The role of the dorsal striatum in reward and decision-making. *J Neurosci* 27:8161–8165.
- Bermudez P, Zatorre RJ. 2005. Differences in gray matter between musicians and nonmusicians. *Ann N Y Acad Sci* 1060:395–399.
- Bullmore E, Sporns O. 2009. Complex brain networks: graph theoretical analysis of structural and functional systems. *Nat Rev Neurosci* 10:186–198.
- Castriota-Scanderbeg A, Hagberg GE, Cerasa A, Committeri G, Galati G, Patria F, et al. 2005. The appreciation of wine by sommeliers: a functional magnetic resonance study of sensory integration. *Neuroimage* 25:570–578.
- David O, Guillemain I, Sallet S, Reyt S, Deransart C, Segebarth C, Depaulis A. 2008. Identifying neural drivers with functional MRI: an electrophysiological validation. *PLoS Biol* 6:2683–2697.
- Delon-Martin C, Plailly J, Fonlupt P, Veyrac A, Royet JP. 2013. Perfumers expertise induces structural reorganization in olfactory brain regions. *Neuroimage* 68:55–62.
- Deshpande G, LaConte S, James G, Peltier S, Hu X. 2009. Multivariate Granger causality analysis of brain networks. *Hum Brain Mapp* 30:1361–1373.
- Deshpande G, Santhanam P, Hu X. 2011. Instantaneous and causal connectivity in resting state brain networks derived from functional MRI data. *Neuroimage* 54:1043–1052.
- Deshpande G, Sathian K, Hu X. 2010a. Assessing and compensating for zero-lag correlation effects in time-lagged Granger causality analysis of fMRI. *IEEE Trans Biomed Eng* 57:1446–1456.
- Deshpande G, Sathian K, Hu X. 2010b. Effect of hemodynamic variability on Granger causality analysis of fMRI. *Neuroimage* 52:884–896.
- Doty RL, Brugger WE, Jurs PC, Orndorff MA, Snyder PJ, Lowry LD. 1978. Intranasal trigeminal stimulation from odorous volatiles: psychometric responses from anosmic and normal humans. *Physiol Behav* 20:175–185.
- Duan X, Long Z, Chen H, Liang D, Qiu L, Huang X, et al. 2014. Functional organization of intrinsic connectivity networks in Chinese-chess experts. *Brain Res* 1558:33–43.
- Frasnelli J, Hummel T, Berg J, Huang G, Doty RL. 2011. Intranasal localizability of odorants: influence of stimulus volume. *Chem Senses* 36:405–410.
- Frisk V, Milner B. 1990. The role of the left hippocampal region in the acquisition and retention of story content. *Neuropsychologia* 28:349–359.
- Friston K, Harrison L, Penny W. 2003. Dynamic causal modeling. *Neuroimage* 19, 1273–1302.
- Glasser MF, Sotiropoulos SN, Wilson JA, Coalson TS, Fischl B, Andersson JL, et al. 2013. The minimal preprocessing pipelines for the Human Connectome Project. *Neuroimage* 80:105–124.
- Granger C. 1969. Investigating causal relations by econometric models and cross-spectral methods. *Econometrica* 37:424–438.
- Grant MM, Wood K, Sreenivasan KR, Wheelock M, White D, Thomas J, et al. 2015. Influence of early life stress on intra- and extra-amygdaloid causal connectivity. *Neuropsychopharmacology* 40:1782–1793.
- Handwerker D, Ollinger J, D'Esposito M. 2004. Variation of BOLD hemodynamic responses across subjects and brain regions and their effects on statistical analyses. *Neuroimage* 21:1639–1651.
- Havlicek M, Friston K, Jan J, Brazdil M, Calhoun V. 2011. Dynamic modeling of neuronal responses in fMRI using curvature Kalman filtering. *Neuroimage* 56:2109–2128.

- He Y, Chen Z, Evans A. 2008. Structural insights into aberrant topological patterns of large-scale cortical networks in Alzheimer's disease. *J Neurosci* 28:4756–4766.
- Hutcherson NL, Sreenivasan KR, Deshpande G, Reid MA, Hadley J, White DM, et al. 2015. Effective connectivity during episodic memory retrieval in schizophrenia participants before and after antipsychotic medication. *Hum Brain Mapp* 36:1442–1457.
- Kim W, Chang Y, Kim J, Seo J, Ryu K, Lee E, et al. 2014. An fMRI study of differences in brain activity among elite, expert, and novice archers at the moment of optimal aiming. *Cogn Behav Neurol* 27:173–182.
- Kolb B, Mychasiuk R, Muhammad A, Gibb R. 2013. Brain plasticity in the developing brain. *Prog Brain Res* 207:35–64.
- Krueger F, Landgraf S, Van der Meer E, Deshpande G, Hu X. 2011. Effective connectivity of the multiplication network: a functional MRI and multivariate Granger causality mapping study. *Hum Brain Mapp* 32:1419–1431.
- Lacey S, Hagtvædt H, Patrick VM, Anderson A, Stilla R, Deshpande G, et al. 2011. Art for reward's sake: visual art recruits the ventral striatum. *Neuroimage* 55:420–433.
- Lotze M, Erhard K, Neumann N, Eickhoff SB, Langner R. 2014. Neural correlates of verbal creativity: differences in resting-state functional connectivity associated with expertise in creative writing. *Front Hum Neurosci* 8:516.
- Lundström BN, Ingvar M, Petersson KM. 2005. The role of precuneus and left inferior frontal cortex during source memory episodic retrieval. *Neuroimage* 27:824–834.
- Luo C, Guo ZW, Lai YX, Liao W, Liu Q, Kendrick KM, et al. 2012. Musical training induces functional plasticity in perceptual and motor networks: insights from resting-state fMRI. *PLoS One* 7:e36568.
- Lutz A, McFarlin DR, Perlman DM, Salomons TV, Davidson RJ. 2013. Altered anterior insula activation during anticipation and experience of painful stimuli in expert meditators. *Neuroimage* 64:538–546.
- McIntosh A, Gozales-Lima F. 1994. Structural equation modeling and its application to network analysis in functional brain imaging. *Hum Brain Mapp* 2:2–22.
- McIntosh AR, Kovacevic N, Lippe S, Garrett D, Grady C, Jirsa V. 2010. The development of a noisy brain. *Arch Ital Biol* 148:323–337.
- Meunier D, Fonlupt P, Saïve AL, Plailly J, Ravel N, Royet JP. 2014. Modular structure of functional networks in olfactory memory. *Neuroimage* 95:264–275.
- Miller BT, D'Esposito M. 2012. Spatial and temporal dynamics of cortical networks engaged in memory encoding and retrieval. *Front Hum Neurosci* 6:109.
- Murphy K, Birn RM, Handwerker DA, Jones TB, Bandettini PA. 2009. The impact of global signal regression on resting state correlations: are anti-correlated networks introduced? *Neuroimage* 44:893–905.
- Oechslin MS, Descloux C, Croquelois A, Chanal J, Van De Ville D, Lazeyras F, James CE. 2013. Hippocampal volume predicts fluid intelligence in musically trained people. *Hippocampus* 23:552–558.
- Onnela JP, Saramaki J, Kertesz J, Kaski K. 2005. Intensity and coherence of motifs in weighted complex networks. *Phys Rev E* 71, 065103.
- Pazart L, Comte A, Magnin E, Millot JL, Moulin T. 2014. An fMRI study on the influence of sommeliers expertise on the integration of flavor. *Front Behav Neurosci* 8:358.
- Pinho AL, de Manzano O, Fransson P, Eriksson H, Ullen F. 2014. Connecting to create: expertise in musical improvisation is associated with increased functional connectivity between pre-motor and prefrontal areas. *J Neurosci* 34:6156–6163.
- Plailly J, Delon-Martin C, Royet JP. 2012. Experience induces functional reorganization in brain regions involved in odor imagery in perfumers. *Hum Brain Mapp* 33:224–234.
- Roebroeck A, Formisano E, Goebel R. 2005. Mapping directed influence over the brain using Granger causality and fMRI. *Neuroimage* 25:230–242.
- Royet JP, Plailly J, Saïve AL, Veyrac A, Delon-Martin C. 2013. The impact of expertise in olfaction. *Front Psychol* 4:928.
- Rubinov M, Sporns O. 2010. Complex network measures of brain connectivity: uses and interpretations. *Neuroimage* 52:1059–1069.
- Saïve AL, Royet JP, Plailly J. 2014. A review on the neural bases of episodic odor memory: from laboratory-based to autobiographical approaches. *Front Behav Neurosci* 8:240.
- Sathian K, Deshpande G, Stilla R. 2013. Neural changes with tactile learning reflect decision-level reweighting of perceptual readout. *J Neurosci* 33:5387–5398.
- Savic I, Gulyas B, Larsson M, Roland P. 2000. Olfactory functions are mediated by parallel and hierarchical processing. *Neuron* 26:735–774.
- Schwarz G. 1978. Estimating the dimension of a model. *Ann Stat* 6:461–464.
- Sporns O, Chialvo DR, Kaiser M, Hilgetag CC. 2004. Organization, development and function of complex brain networks. *Trends Cogn Sci* 8:418–425.
- Tzourio-Mazoyer N, Landeau B, Papathanassiou D, Crivello F, Etard O, Delcroix N, et al. 2002. Automated Anatomical Labeling of activations in SPM using a macroscopic anatomical parcellation of the MNI MRI single-subject brain. *Neuroimage* 15:273–289.
- Valkanova V, Eguia Rodriguez R, Ebmeier KP. 2014. Mind over matter—what do we know about neuroplasticity in adults? *Int Psychogeriatr* 26:891–909.
- Van den Heuvel MP, Stam CJ, Boersma M, Hulshoff Pol HE. 2008. Small-world and scale-free organization of voxel based resting-state functional connectivity in the human brain. *Neuroimage* 43:528–539.
- Van den Heuvel MP, Stam CJ, Kahn RS, Hulshoff Pol HE. 2009. Efficiency of functional brain networks and intellectual performance. *J Neurosci* 29:7619–7624.
- Voss MW, Prakash RS, Erickson KI, Basak C, Chaddock L, Kim JS, et al. 2010. Plasticity of brain networks in a randomized intervention trial of exercise training in older adults. *Front Aging Neurosci* 2:32.
- Watts DJ, Strogatz SH. 1998. Collective dynamics of 'small-world' networks. *Nature* 393:440–442.
- Xia M, Wang J, He Y. 2013. BrainNet Viewer: a network visualization tool for human brain connectomics. *PLoS One* 8:e68910.

Address correspondence to:

*Dietmar Cordes*

*Cleveland Clinic Lou Ruvo Center for Brain Health*

*888 West Bonneville Avenue*

*Las Vegas, NV 89106*

*E-mail: cordesd@ccf.org*